SHADOW DETECTION IN HYPERSPECTRAL IMAGES ACQUIRED BY UAV

N. N. Imai [1], A. M. G. Tommaselli [1], A. Berveglieri [1], E. A. S. Moriya [1]
[1] UNESP, School of Science and Technology, 19060-900 Presidente Prudente, Brazil - (nilton.imai, a.berveglieri, a.tommaselli)@unesp.br, erikaasaito@gmail.com

Commission III, WG III/4

KEY WORDS: Shadow detection, UAV, hyperspectral image, high spatial and spectral resolution image, spectral signatures, cloud shadow in agricultural fields.

ABSTRACT:

Shadows are common in any kind of remote sensing images. Unmanned Aerial Vehicle – UAV with a light camera attached can acquire images illuminated either by direct sunlight or by diffuse light under clouds. Indeed, areas with pixels shaded by clouds must be detected and labelled in order to use this additional information for image analysis. Classification of health and diseased plants in permanent culture as the orange plantation field can present some errors due to tree cast shadow. So, hyperspectral or multispectral image classification can be improved by previous shadow detection. Some FPI hyperspectral camera, designed for agricultural applications is limited in the spectral range between 500 to 900 nm. Wavelengths in the region of blue light and in the SWIR spectral region have physical properties that enable the enhancement of shaded regions in the images. In this work some combinations of different spectral bands were evaluated in order to specify those suitable to detect shadows in agricultural field images. In this sense, considering that vegetation and soil are the two main kind of coverage in an agricultural field, we hypothesized that wavelengths near blue light and the longest near infrared available in the camera range are good choices. In both spectral regions soil and vegetation targets have small spectral differences which contribute to enhance the differences between shaded and illuminated regions in the image. Hyperspectral images acquired with a FPI hyperspectral camera onboard a UAV over a plantation of oranges were used to evaluate these spectral bands. The results showed that the wavelengths of aproximatelly 510 nm and 840 nm available in the FPI camera are the best to detect any type of shadows in the agricultural fields.

1. INTRODUCTION

There are shadows in almost all types of aerial imagery. Shadows in images occlude other targets and limit spectral analysis, so that their identification and characterization can help image analysis. They are useful when estimating Sun orientation, estimating or measuring objects size and for some non-linear radiometric corrections. However, there are problems in some kinds of image analysis such as object detection or recognition, image matching, spectral signature analysis among others.

Even considering that shadows could provide useful information in many kind of image analysis, they frequently cause errors in the image classification and analysis process. Image analysis can be improved by shadows previous detection and labelling since targets can be partially occluded by them. Either way, its location must be known in order to take advantage of its presence in the image or to prevent image analysis errors.

High resolution images taken by Unmanned Aerial Vehicle – UAV with a light camera attached can have areas with pixels of targets either directly illuminated by the sunlight or by diffuse light in shaded areas. Cloud shaded pixels cannot be analysed by the same parameters as regular directly sun illuminated targets. There are alternatives to analyse these classes of cloud shaded pixels. Another alternative is to repeat the image collection in the same region to have pixels free from cloud shadow influence. However, in both cases it is necessary to detect which pixels are influenced by cloud shadows.

Many works were developed in order to detect shadows in remote sensing images and there are many improvements related to the cloud shadow detection in orbital remote sensing images (Sun et al., 2018; Zhu et al., 2015; Simpson et al., 2000). Dare (2005) applied a variance-based region filtering in order to separate shadows from falsely detected non-shadowed regions. This approach was adopted to avoid targets which have radiometric properties similar to shadows, namely water, trees and dark elements.

There are many algorithms dedicated to shadow detection: some approaches are based on spectral scattering, which should be stronger in lower wavelengths, mainly in the blue channel while some others are based on combination of radiometric and geometric analysis or based on dark objects segmentation.

Shadow detection algorithm in color aerial images was also developed by Freitas et al., 2017 and Santos et al. (2006). Freitas et al. (2017) developed an algorithm based on the hypothesis that most deep shadows have blue and violet wavelengths (Adler-Golden et al., 2002; Polidorio et al., 2003). They computed an index previously proposed by Polidorio et al. (2003), which is computed using the intensity and saturation components from HIS color space in order to take advantage of the stronger scattering in the violet and blue wavelengths. Shadow pixels have low intensity but high saturation of the visible scattered light. Freitas et al. (2017) combined that index with a shadow filter as proposed by Santos et al. (2006) in order to detect shaded pixels.

Spectral regions in the blue light and SWIR are usually adopted for shadow detection, but FPI camera designed for agricultural applications does not acquire blue light or SWIR wavelengths. in different spectral ranges. Rikola camera is a hyperspectral camera based on the Fabry-Pérot Interferometer (FPI). Spectral bands are set according to the designed mission. The central

wavelength of each band is adjustable based on a distance between mirrors of the FPI device. Even being feasible to choose up to 50 narrow bands in this camera, it is common to specify only 25 bands for agricultural applications. In any case, it is useful selecting and evaluating which bands are more suitable for shadow detection, considering the spectral range from 500 nm to 900 nm of this kind of FPI camera.

This work aims to select spectral bands from the region of visible and near infrared to identify the pixels influenced by shadow in agricultural fields. Summer harvest monitoring is an important application for remote sensing based on UAV technology, but cloud shadows may introduce undesirable noise that should be avoided in order to have a useful mosaic for image analysis.

We have hypothesised that there are few wavelengths in the FPI hyperspectral image which are able to better discriminate shaded areas. Indeed, in agricultural fields there are mainly vegetation cover and soil which can be covered by shadows. Then, shadow detection can be simplified since the spectral signature was considered in order to simplify the classification process. It is well known that many spectral indices take advantage of their spectral signature in order to enhance their differences. Some cameras are designed to take multispectral images for agricultural applications having spectral bands in the red and near infrared regions.

The combination between red and near infrared regions must be avoided to facilitate shadow detection since that these spectral regions enhance differences between soil and vegetation. Longer wavelengths in the near infrared can have soil reflectance as high as vegetation cover and small wavelengths radiation in the visible region can have low reflectance for both types of cover. In this work we adopted two samples of images: with and without cloud shadows, in order to evaluate the performance of two spectral bands among 25 spectral bands to shadow detection. One is in the spectral region in the blue and green spectral regions and other is the longest wavelength in the near infrared taken by our FPI camera.

Two sample sets of hyperspectral images acquired by a tunable Fabry-Pérot interferometer camera developed by the VTT Technical Research Centre of Finland were adopted to select spectral bands suitable to classify pixels affected by shadows. An unsupervised classification, with K means algorithm, was applied in order to classify cloud shadows, plant shadows and illuminated regions in images which Ground Sample Distance – GSD varies between 10 cm to 50 cm. We applied this basic algorithm in order to check the similarities between soil and vegetation spectra in the shaded regions and between illuminated and shaded regions.

1.1 Cloud shadows and plant shadows in agricultural fields

There are two classes of shadows: cast and self shadows. The former is a result of the projection of the object and the latter is a projection of shadows on the own object. In this work both kinds of shadows are considered together. Classification of health and diseased plants in permanent culture as the orange plant field can present some errors due to tree cast shadow. Aerial surveying which acquire images from sunlighted regions and cloud shaded regions could not produce a well radiometrically calibrated mosaic. And so, these kind of images are not suitable for quantitative analysis.

Umbra and penumbra are two important shadow classes since they obscure the scene in different degrees. Umbra is a region of shadow where the irradiance of surface depends on scattered light. Penumbra is a region with shadows near the border where shadows usually have higher intensity values than umbra due to the adjacent sources of light. Cloud shadows usually have both types: umbra in the centre and penumbra in the border, but penumbra can also occurs inside the shadow region due to the cloud density variation. Additionally, cloud shadows have differences on their darkness levels.

Cloudiness variations cause illumination variations, since cloud shadows can block sunlight partially or totally, producing a mosaic of umbra and penumbra. This kind of shadow is more complex so that solution to recover information from the shaded area is an important research topic for UAV image processing and analysis. Radiometric compensation of different degrees of illumination among images is one of the primary tasks to produce mosaics. The radiometric compensation of images taken under the same illumination conditions is a usual task, however, this radiometric compensation in a set of images with and without cloud shadows influences is more difficult to solve.

Summer crop monitoring is an important application for UAV images, but the image analysis depends on the spectral data quality. There is a high probability of having directly illuminated and diffusely illuminated targets in an aerial survey based on UAV during the summer crop in Brazil. Indeed, this is a difficult task in image analysis since the agricultural fields in Brazil are usually large. The application of different algorithms on illuminated regions and shaded by clouds should produce better mosaics.

Classification of tree species in a scene of natural forest area based on a tree crown analysis can also be benefited by preliminary self shadow detection. Stressed orange trees can be identified in multispectral and hyperspectral images, but previous self shadow detection can be useful for the image analysis. In both cases, previous shadow detection can add this important feature to the analysis.

1.2 Fabry-Pérot Interferometer (FPI) hyperspectral camera

There are many light image sensors developed to acquire multispectral and hyperspectral images to produce crop images. The hyperspectral camera based on Piezoactuated FPI camera is a light camera designed to get images onboard a UAV.

Figure 1. Hyperspectral camera based on a Piezoactuated FPI

The camera adopted in this work is a 2014 prototype, model DT-0014 (Figure 1), developed by VTT (Technical Research Center of Finland) and Rikola Ltd. The more suitable model for crop monitoring has its spectral range between 500 nm to 900 nm.

1.3 Vegetation and soil spectral signatures

Agricultural field images collected by light cameras attached to a UAV have vegetation cover as the main target, but soil is a natural background which is also visible in a variable degree depending on the harvest phenological stage. Anyway, these kinds of image have both classes of targets combined. Then, it is desirable they have lower spectral reflectance differences in the wavelengths adopted to detect pixels which are influenced by shadows and consequently enhance the contrast between pixels which correspond to sunlighted regions in contrast with shaded regions.

An examination of typical spectral signatures of soil (Fig. 1) and vegetation (Fig.2) in the spectral range from 500 nm to 900 nm, shows that wavelengths at the limits of this range are suitable to shadow detection in the images of agricultural field. In Fig. 2 red lines show that the differences of the spectral signatures of soil and vegetation tend to be lower. Indeed, these spectral signatures depend on many variables, including degree of humidity, but they tend to oscillate around these typical signatures.

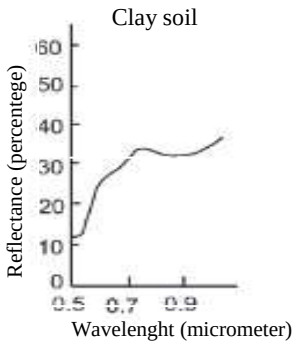

Figure 1: Spectral response of soils
Adapted from McCoy, 2005

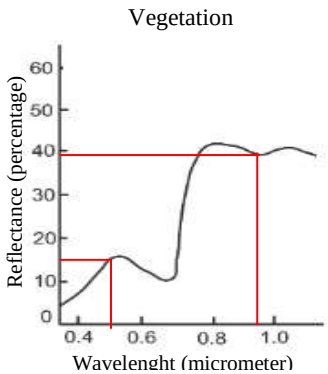

Figure 2: Spectral response of vegetation
Adapted from McCoy, 2005

2. MATERIALS AND METHODOLOGY

Segments of two mosaics were adopted as sample images to evaluate our hypothesis. One mosaic was produced by an aerial surveying with a light aircraft with a flight height of approximately 800 m, and another produced by a UAV platform with a flight height of approximately 120 m. The first survey produced a spectral cube which pixels have Ground Sample Distance - GSD of 50 cm, from here named LRcube (low resolution cube) and the second a cube with 10 cm of GSD, which is named as HRcube (high resolution cube). Both cubes have 25 spectral bands. LRcube is a digital number-DN mosaic, while HRcube is a Reflectance Factor mosaic produced by radiometric calibration process (Honkavaara et al., 2012; 2013).

We adopted these two types of spectral data in order to evaluate the robustness of the spectral classification applied on a radiometric calibrated and non-calibrated data sets. This is an important aspect for real time shadow cloud detection approaches.

Table 1 shows the central wavelength and FWHM of both cubes. Two different plots of the same orange-producing farm located in Santa Cruz do Rio Pardo, state of São Paulo, Brazil were covered.

Figure 3 shows the location of this area. The coordinates of the study area in the WGS84 system are 22°47'42.14"S and 49°23'46.28"W.

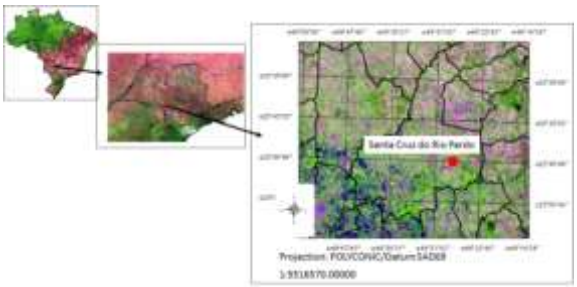

Figure 3. Guacho farm in the city of Santa Cruz do Rio Pardo. City of Santa Cruz do Rio Pardo in Sao Paulo State and in Brazil.

Table 1 shows the central wavelengths and their Full width at half maximum-FWHM for both spectral cubes.

Table 1 - Central wavelenghts and their FWHM for 50 cm GSD and 10 cm spectral cubes

λ (nm)	FWHM (nm)	λ (nm)	FWHM (nm)	λ (nm)	FWHM (nm)
506.1	12.5	629.9	15.2	734.8	19.8
519.9	17.4	650.4	14.7	750.2	18
535.1	16.8	660.5	17.1	769.9	18.7
550.4	16.5	669.7	19.8	790.30	17.4
563.9	17.1	690.3	18.9	810.5	18
580.2	16	700.3	18.9	819.7	17.8
590.0	16.6	715.1	19.7	830.2	16.8
605.1	15.1	725.1	19.1	840.3	16.7
620.2	16.3	λ = central wavelength			

The evaluation of the hypothesis of this work was based on statistics extracted from a sample of pixels influenced by shadows, in order to check their spectral similarities and differences. In this sense, we have applied an unsupervised classification algorithm, K-means, since it is expected that pixels of shaded regions are spectrally different from those non-shaded (sun lighted) regions. In addition, there is no intention to propose an algorithm for shadow detection, but rather

evaluating our hypothesis which can be useful for further algorithm design.
Maximum, minimum and mean values are enough to check our hypothesis. The range between maximum and minimum values along the spectral range must be lower at the limits of the camera spectral range.

Only these two wavelengths at the limits of the camera spectral range were adopted to shadow classification. The spectral classes produced were examined in order to check which one was related to shaded regions. Then, pixels belonging to this spectral class are adopted as a region of interest which produced the statistics of the shadow pixels in each spectral cube.

3. RESULTS

The images which central wavelengths are 506.1 nm and 840.3 nm were adopted as the first option for shadow classification. These bands were visually evaluated in order to check their quality, since the sensibility at the limits of the spectral range is low and images can have low quality depending on the irradiance of the targets and the integration time when acquiring the hypercubes.

Only the images of the LRcube have good quality for both wavelengths, while the lower wavelength image of HRcube presented high level of noise. So, it was necessary to adopt the spectral image which central wavelength is 519.9 nm instead of 506.1 nm. The quality of the spectral image centred at 840.3 nm presented good quality in both spectral cubes.

Figure 4 shows a color composition adopting the central wavelengths images 840.3 nm to red - R, 660.5 nm to green - G and 506.1 nm to blue - B. The 660.5 nm were presented as green to increase the contrast of the dirt road which is inside the cloud shadow. This is not a good choice to detect shadow due to the high contrast between vegetation and dirt road in this spectral image. It is noted that the contrast between the dirt road and vegetation is lower in the Fig. 3 color composition which was produced by combining the 840.3 nm to the 506.1 nm avoiding the image which central wavelength is 660.5 nm.

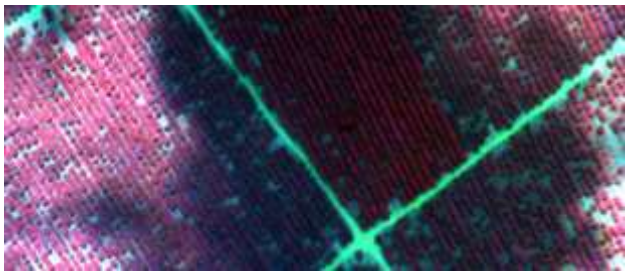

Figure 4. Color composition of LRcube: R 840.3 nm, G 660.5 nm and B 506.1 nm

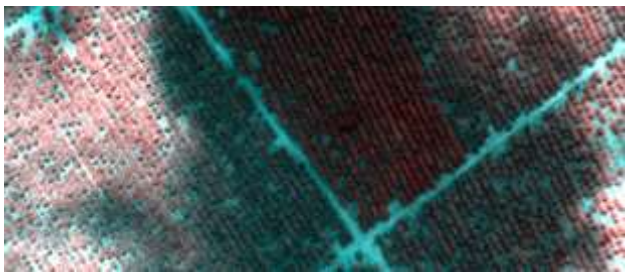

Figure 5. Color composition of LRcube: R840.3 nm, G 840.3 nm and B 506.1 nm

The LRcube was adopted in order to have cloud shadow and self shadows in the same cube. The HRcube is showed in a Fig. 6 where there are only shadows of the orange plats. There are some parts of dirt road under the shaded areas and out of shadow. Two bands of HRcube are showed as a color composition in Fig. 6, where 840.3 nm is the R and G component while 519.9 nm is represented as B.

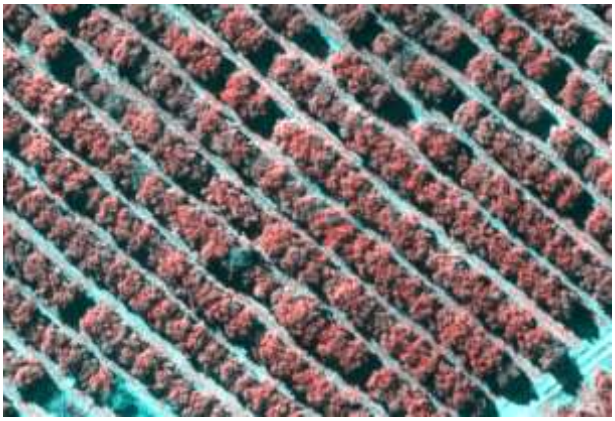

Figure 6. Color composition of HRcube: R 840.3 nm, G 519.9 nm and B 519.9 nm

Figure 7 shows the best result for the LRcube classification adopting images whose central wavelengths are 840.3 nm and 506.1 nm. Classification result includes shadows of orange plants and cloud shadow. It can be noticed that the result presents few errors despite the algorithm is a simple clustering technique based only on a spectral feature. The results obtained seem to be a suitable sample data to extract statistics of the shadow pixels.

Figure 7. The classification results of two bands of the LRcube where red are pixels of shadows which include plant shadows and cloud shadows while green represents pixels of the non-shadow areas.

The classification of two bands of the HRcube is shown in Fig. 8, where red colour depicts pixels of shaded regions and other colours represents the spectral variations of vegetation coverage.

This cube has 10 cm GSD which is a very high spatial resolution. Vegetation is classified into different spectral classes due to different densities, health and kind of vegetation. This result also demonstrates that the spectral feature analysis is good enough to detect pixels with shadows and it seems to be suitable to be adopted as a sample data to extract statistics for our analysis.

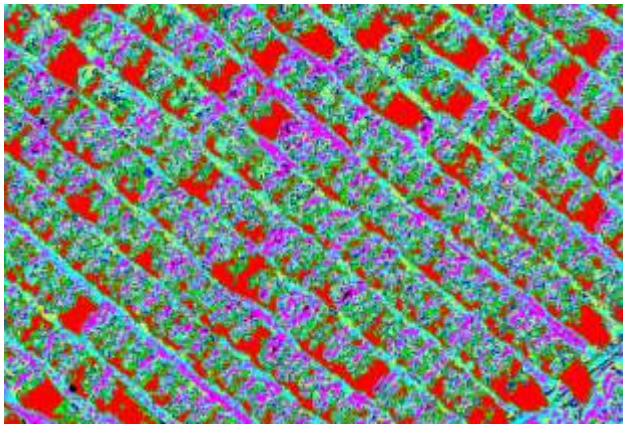

Figure 8. The classification results of two bands of the HRcube where red are pixels of shadows while other colors represent pixels of the no shadow areas.

Figure 9 and 10 show segments of LRcube and HRcube color compositions overlapped by the polygons of respective classified shadows.

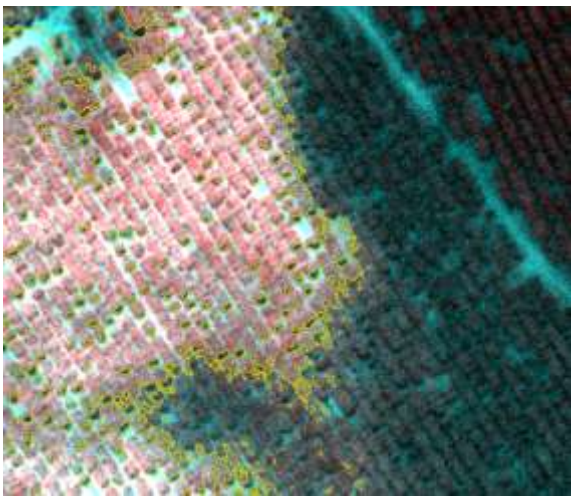

Figure 9. Image sample of LRcube color composition overlapped to the polygons which represent shadow

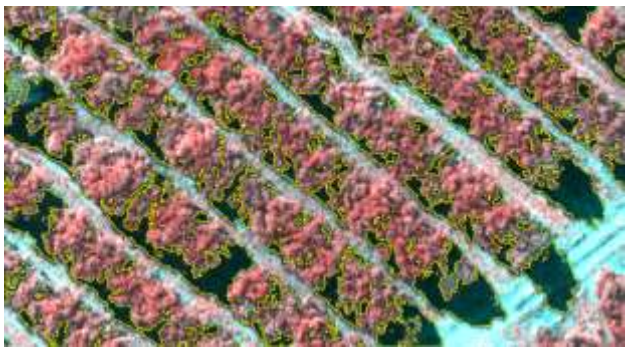

Figure 10. Image sample of HRcube color composition overlapped to the polygons which represent shadow

Figures 11 and 12 present graphics of the maximum, minimum and mean values extracted from both samples.

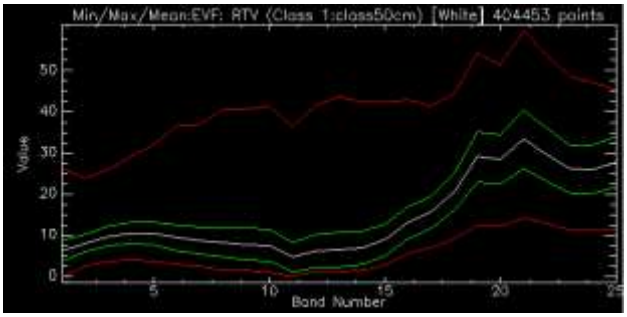

Figure 11. Graphical representation of maximum, minimum (red lines) and mean (white) values of all wavelengths of the sample which represents shadow pixels in the LRcube

It is possible to verify that the difference between maximum and minimum values tends to be lower at the limits of the spectral wavelengths of the camera. In fact, the band centred at 519.9 nm has the minimum difference in the visible spectral region.

The statistics of this spectral band is minimun equal to 2.535, maximum equal to 23.903, mean value is 7.949 and the standard deviation is 2.145. While the band centred at 840.3 nm has the minimum difference in the near infrared where the statistics values are: 11.677 as minimum, 45.383 as maximum, mean is 28.001 and the standard deviation is equal to 6.171. It is noted that the band centred at 519.9 is a little bit better than the band adopted to classify the shaded areas, but the sample extracted from the cube was suitable to show that the extremes of the available spectra are good choices for shadow detection.

Figure 12 is similar to Figure 11 but represents the statistics of the HRcube. It is noted that the curves of maximum values are similar for both cubes, while mean and minimum values do not vary similarly. This behaviour could be related to the lower radiation available since there are not scattered light but mostly from adjacency, which seems to be very low.

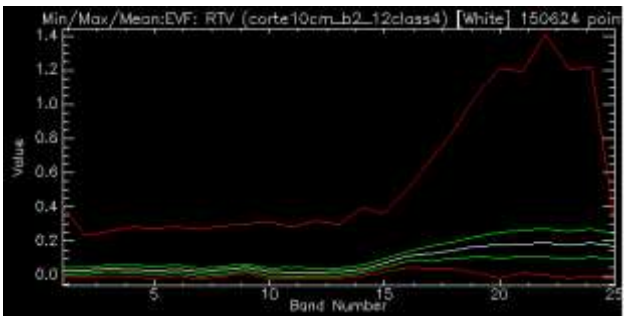

Figure 12. Graphical representation of maximum, minimum (red lines) and mean (white) values of all wavelengths of the sample which represent shadow pixels in the LRcube

Lower differences between maximum and minimum values are on 519.9 nm and on the 840.3 nm, as well as to the LRcube. All statistics values are presented in the appendix.

4. CONCLUSION

Sample pixels of shadows were extracted from two spectral cubes by applying K-means adopting only 2 bands from 25 bands available in a cube produced by FPI hyperspectral camera. These two bands were chosen at the limits of the spectral range available, one in the visible spectral range and another at the longest wavelength of the both cubes.

The accuracy of classified shaded regions can be considered good based only on a visual evaluation, since that the pixels of the samples do not need high accuracy to be adopted as sample data for statistical analysis.

The analysis of the statistics of both sample pixels showed that the hypothesis that bands centred at the limits of the spectral range of FPI camera is a good choice for shadow detection. However, the band centred at 519.9 nm is better than the smallest wavelength, 506.1 nm, which was indicated as the best choice.

5. REFERENCES

Adler-Golden, S. M., Matthew, M. W., Anderson, G. P., Felde, G. W. and Gardner, J. A. 2002. Algorithm for de-Shadowing Spectral Imagery. In: Proceedings of SPIE, *Imaging Spectrometry VIII*, v. 4816, pp.203-210. Seattle: USA. doi:10.1117/12.451691.

Dare, P. M. 2005. Shadow Analysis in High-Resolution Satellite Imagery of Urban Areas. *Photogrammetric Engineering and Remote Sensing*, 71(2), 169-77.

Freitas, V. L. S., Reis, B. M. F., Tommaselli, A. M. G. 2017. Automatic shadow detection in aerial and terrestrial images. *Bulletin of Geodetic Sciences*, 23(4), 578-590. http://dx.doi.org/10.1590/S1982-21702017000400038

Honkavaara, E.; Kaivosoja, J.; Mäkynen, J.; Pellikka, I.; Pesonen, L.; Saari, H.; Salo, H.; Hakala, T.; Markelin, L.; Rosnell, T., 2012. Hyperspectral reflectance signatures and point clouds for precision agriculture by light weight UAV imaging system. In: *ISPRS Annals of the Photogrammetry, Remote Sensing and Spatial Sciences*, v. I-7, 2012, XXII ISPRS Congress, 25 august-01 september 2012, Melbourne, pp.353-358.

Honkavaara, E.; Saari, H.; Kaivosoja, J.; Pölönen, I.; Hakala, T.; Litkey, P.; Mäkynen, J.; Pesonen, L., 2013. Processing and assessmet of spectrometric, stereoscopic imagery collected using a lightweight UAV Spectral Camera for Precision Agriculture. *Remote Sensing* 5, pp. 5006-5039.

Simpson, J. J., Jin, J., and Stitt, J. R. 2000. Cloud Shadow Detection Under Arbitrary Viewing and Illumination Conditions. *IEEE TRANSACTIONS ON GEOSCIENCE AND REMOTE SENSING*, 38(2), 972-976.

Sun, L., Liu, X., Yang, Y., Chen, T.T., Wang, Q., Zhou, X. 2018. A cloud shadow detection method combined with cloud height iteration and spectral analysis for Landsat 8 OLI data. *ISPRS Journal of Photogrammetry and Remote Sensing*, 138 (2018) 193–207. https://doi.org/10.1016/j.isprsjprs.2018.02.016

Polidorio, A. M., Flores F. C., Imai N. N., Tommaselli, A. M. G. and Franco, C. 2003. Automatic Shadow Segmentation in Aerial Color Images. In: Proceedings of the XVI SIBGRAPI. *XVI Brazilian Symposium on Computer Graphics and Image Processing*. São Carlos, Brasil, 12-15 October 2003. doi:10.1109/SIBGRA.2003.1241019.

Santos, D., Dalmolin, Q. and Basso, M. A. 2006. Detecção Automática de Sombras em Imagens de Alta Resolução. *Bulletin of Geodetic Sciences*, 12(1), pp.87-99. http://ojs.c3sl.ufpr.br/ojs2/index.php/bcg/article/view/5310/3931.

Zhu, Z., Woodcock, C. E. 2011. Object-based cloud and cloud shadow detection in Landsat imagery. *Remote Sensing of Environment*, 118 (2012) 83–94. doi:10.1016/j.rse.2011.10.028

ACKNOWLEDGEMENTS

This research has been jointly funded by the São Paulo Research Foundation (FAPESP – grant 2013/50426-4) and Academy of Finland – decision number 273806). We are also thankful to Foundation for Unesp development (Fundunesp), Agroterenas Citros, Branco Peres Agribusiness, Cambuhy Agrícola, Citrosuco, Faro Capital Agribusiness, for funding this research; and to the FAPESP who supported us for the participation in the Geospatial Week 2019.

Appendix

Statistics of the pixels of shaded regions – LRcube

band	Min	Max	Mean	Stdev
Band_1	0.0190	26.4127	6.1582	2.5664
Band_2	2.5349	23.9034	7.9497	2.1454
Band_3	3.6931	25.9973	9.7329	2.4040
Band_4	3.8026	29.1708	10.4711	2.6478
Band_5	3.6614	31.8437	10.4057	2.8372
Band_6	3.0447	36.6894	9.3988	3.1341
Band_7	2.4837	36.9510	8.6872	3.2646
Band_8	1.3258	40.6287	8.2507	3.5194
Band_9	1.4794	40.5925	7.7677	3.7783
Band_10	0.9379	41.4401	7.4866	3.9121
Band_11	0.000	36.4799	4.6394	3.6270
Band_12	1.0887	41.6804	6.1327	3.9682
Band_13	1.1039	43.6104	6.4758	4.1843
Band_14	1.4975	42.2491	6.9054	3.9331
Band_15	2.6684	42.3588	8.8897	3.8775
Band_16	5.7421	42.8044	13.0557	3.8777
Band_17	6.8236	41.2510	15.5842	3.8509
Band_18	9.1865	44.7122	20.7432	4.5255
Band_19	12.2939	54.3787	29.0793	6.1464
Band_20	12.2472	51.3073	28.4814	6.0136
Band_21	14.1191	59.6971	33.3299	7.1396
Band_22	12.9550	53.9740	29.6363	6.5185
Band_23	11.2555	48.5833	26.0962	5.8302
Band_24	11.1881	47.1272	25.9845	5.8066
Band_25	11.6773	45.3831	28.0006	6.1707

Statistics of the pixels of shaded regions – HRcube

Band	Min	Max	Mean	Stdev
1	0.0000	0.2392	0.0286	0.0199
2	0.0000	0.1928	0.0344	0.0156

3	0.0000	0.2324	0.0401	0.0166
4	0.0000	0.2822	0.0435	0.0177
5	0.0000	0.2874	0.0436	0.0183
6	0.0000	0.2612	0.0384	0.0177
7	0.0000	0.2931	0.0396	0.0189
8	0.0000	0.2755	0.0361	0.0183
9	0.0138	0.3004	0.0464	0.0173
10	0.0000	0.3021	0.0355	0.0196
11	0.0000	0.2927	0.0387	0.0237
12	0.0000	0.2944	0.0314	0.0185
13	0.0000	0.2598	0.0316	0.0179
14	0.0000	0.2740	0.0356	0.0186
15	0.0248	0.3407	0.0681	0.0195
16	0.0503	0.5028	0.1057	0.0242
17	0.0429	0.5939	0.1195	0.0311
18	0.0408	0.7600	0.1290	0.0377
19	0.0186	0.9857	0.1461	0.0474
20	0.0000	1.2249	0.1670	0.0561
21	0.0134	1.1576	0.1575	0.0589
22	0.0052	1.0847	0.1613	0.0608
23	0.0000	1.0419	0.1606	0.0628
24	0.0000	0.9622	0.1653	0.0632
25	0.0000	0.0844	0.1549	0.0565